RESEARCH ARTICLE

ADVANCED OPTICAL MATERIALS
www.advopticalmat.de

Fast and Reversible Red Emission Modulation in Photoswitchable Molecules Toward Optical Data Storage

*Pankaj Dharpure, Heyou Zhang, Zifei Chen, Max Gießübel, Paul Mulvaney, Jürgen Köhler, and Mukundan Thelakkat**

Photoswitchable dithienylperfluorocyclopentene (DCP) and dibenzothienylperfluorocyclo-pentene dioxide (BTCPO4) have potential applications in optical data storage. They exhibit high fatigue resistance and reverse ON-OFF photoswitching of emission due to ring opening and closing reactions, feasible at two different wavelengths. DCPs are non-emissive in both the open and closed states, whereas BTCPO4s are emissive upon ring closure. There is a scarcity of fast, reversible, and bistable photoswitchable red emitters. Therefore, a series of red-emitting BTCPO4s is synthesized, and their detailed photophysical characterization is reported here.
This study shows that the red emitters are highly stable in the cyclized form, requiring high laser power and long irradiation times for reverse cyclization to the non-emissive state. Also, the ON-OFF contrast ratio is very low. To enable red emission modulation and to increase the contrast ratio, energy transfer from the red-emitting BTCPO4 isomer to a fast photoswitchable non-emitting DCP molecule is exploited. This novel approach enables 60 times faster, reversible modulation of the red emission with a four times higher contrast ratio (≈90%) and at 150 times lower visible laser irradiation intensity than can be achieved for the pure red emitter alone. Finally, the potential for optical data storage is demonstrated for 100 write-read-erase cycles.

1. Introduction

The advantages of fluorescent molecules have been well documented in a variety of applications, such as bioimaging and optical data storage, and display.[1–5] Photoswitchable fluorescent molecules have the unique property that their emission can be switched ON and OFF upon photoirradiation with two different wavelengths of light. A variety of photoswitchable molecular systems comprising photoswitches such as azobenzenes, spiropyran, acyl hydrazones, and diarylethenes, or their dyads containing fluorophores such as perylenebisamide, coumarins, and rhodamines have been explored because of their unique reversible photoswitching and fatigue resistance properties.[6–13] Among these candidates, dithienylperfluorocyclopentenes (DCPs), constitute one very promising class of multicolor photoswitchable molecules, which exhibit high thermal stability and rapid response time to photo-irradiation with a suitable wavelength of light (UV/Vis). They were first reported by Irie and coworkers.[14–17] DCPs can be repeatedly switched for multiple cycles without a significant decrease in the contrast ratio (due to their high fatigue resistance).[18] A key reason for this is that DCP photoswitches undergo only small structural changes when converting between the different isomers. This, in turn, is due to facile 6π electron cyclization and reverse cyclization. This small steric requirement for both ring opening and closing enables the photoswitching of DCPs to be equally efficient in both solution and in compact solid-state (crystalline state).[16,17] However, the fast photoswitchable DCP molecules were non-fluorescent in both the open and closed forms, shown as DCP (a) and DCP (b) in **Scheme 1**a.[14] Hence, it was necessary for the non-fluorescent DCP molecules to be covalently linked to, or mixed with, a fluorescent dye in order to exploit the full potential of DCPs for fluorescence modulation applications. This strategy allowed the modulation of dye emission (ON-OFF) by energy transfer, both in single molecules as well as in ensembles.[19–29] A breakthrough in the synthesis of turn-on photoswitches was subsequently reported by Kim and co-workers, who utilized the oxidation of sulfur atoms in dibenzothienylperfluorocyclopentenes (BTCP) to fluorescent sulfones (BTCPO4).[30] Further, Irie and others systematically explored a series of intrinsic fluorescent BTCPO4 molecules with

P. Dharpure, M. Thelakkat
Applied Functional Polymers
University of Bayreuth
95440 Bayreuth, Germany
E-mail: mukundan.thelakkat@uni-bayreuth.de
H. Zhang, M. Gießübel, J. Köhler
Spectroscopy of Soft Matter, University of Bayreuth
95440 Bayreuth, Germany
Z. Chen, P. Mulvaney
ARC Centre of Excellence in Exciton Science
School of Chemistry
University of Melbourne
Parkville, VIC 3010, Australia
J. Köhler, M. Thelakkat
Bavarian Polymer Institute (BPI) and Bayreuther Institut für Makromolekülforschung (BIMF)
University of Bayreuth
95440 Bayreuth, Germany
The ORCID identification number(s) for the author(s) of this article can be found under https://doi.org/10.1002/adom.202502406

DOI: 10.1002/adom.202502406

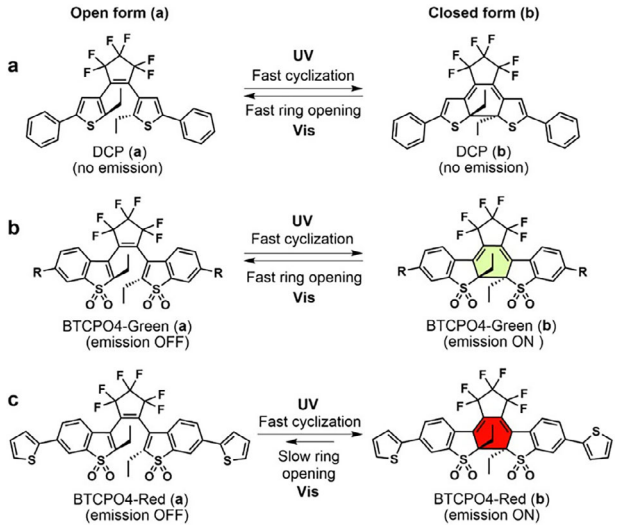

Scheme 1. Photochroism of DCP and BTCPO4. DCP is non-emitting in both isomeric forms, whereas BTCPO4 emits on ring closure and is called a turn-on photoswitch.

various aryl substitutions at 6,6' position.[31–37] These intrinsically green-emitting molecules are termed BTCPO4-Green (a) or (b) and are shown in Scheme 1b. These green emitters have negligible emission in the open state (a) but are highly emissive in the closed state (b). They also exhibit high thermal stability, fast reversible photoswitching in both directions, and high fatigue resistance.[32–35] However, the fast reversible photoswitching of this class of intrinsic fluorescent molecules has been limited to green color emission up to now.

Red-emitting $BTCPO_4$ compounds exhibit exceptional photostability under both ultraviolet (UV) and visible light irradiation, making them superior to conventional red-emitting dyes for long-term optical applications. In a comparative study led by Prof. Irie, $BTCPO_4$ demonstrated significantly greater photostability than commonly used dyes such as Rhodamine 101 and Fluorescein when exposed to UV light (365 nm) and visible light (>440 nm).[31] This enhanced stability positions $BTCPO_4$ as a promising candidate for applications requiring sustained fluorescence performance. However, in the case of red-emitting BTCPO4s, unlike the green emitters, reverse cyclization of the closed form BTCPO4-Red (**b**) to an open form (**a**) is very hard to achieve in most cases, and it usually requires a very high light intensity (up to 120 kW cm^{-2}) (Scheme 1c).[38] The slow reverse cyclization rate is due to the extra stability of the closed form isomer, provided by the extended π-electron delocalization and intramolecular charge transfer.[39–41] The reverse cyclization of BTCPO4-Red from closed form (b) to open form (a) (Scheme 1c) can be improved considerably by replacing the ethyl group with the sterically crowded neopentyl group at the reactive carbon.[42] Although the synthesis of $BTCPO_4$ molecules containing the neopentyl group has been reported for all-visible-light photoswitching, their potential applications in write-read-erasing data storage (as reported here) have not yet been explored. Recently, a two-photon absorption strategy was reported to improve the reverse cyclization of BTCPO4-Red, from closed form (**b**) to open form (**a**). However, this strategy likewise required high-power excitation pulses to drive two-photon absorption.[43] In summary, this class of red-emitting photostable BTCPO4s exhibits fast cyclization reaction (emission turn-on) but faces two issues: a slow reverse cyclization reaction (emission turn-off) and the requirement of very high visible light intensities. This restricts the use of these red-emitting BTCPO4s molecules to any application where fast photoswitching in both directions is required. Low-intensity light irradiation is a prerequisite in general for optical data storage and encryption to avoid sample degradation, light scattering, and light interference problems. Specifically, light scattering and light interference reduce the signal-to-noise ratio, thus badly influencing the data read-out accuracy. Additionally, these effects increase the cross-talk between the two neighboring data points, further degrading data fidelity. While working on optical data encryption using green-emitting $BTCPO_4$ embedded in polystyrene (PS) beads (300 nm diameter) arranged in an ordered array with 5 µm spacing on a compact 0.5 cm × 0.5 cm glass substrate, we observed that the intensity of light irradiation plays a critical role in the fidelity of information writing, reading, and erasing.[44] High-intensity light ($>$ 3 W cm^{-2}) leads to light scattering results in a cross-talk between two neighboring data points, compromising data integrity, especially in miniaturized systems (scattering can be seen in the videos of the Ref article).[44] Thus, to increase the data readability accuracy further, low-intensity UV and visible light irradiation is essential.

In this study, we address the issue of reversible fast photoswitching of red emitters. This is a key step toward accessing the full potential of multiple color photoswitching to advance optical data encryption further. We synthesized a variety of red emitters and studied the emission quenching via reverse cyclization. To address the challenges of low contrast ratio and the need for high visible light intensities, we prepared polymer blends with fast photoswitchable DCP molecules, which enabled energy transfer (FRET or radiative energy transfer) at low laser intensities for a variety of red emitters. This constitutes a general and novel strategy for overcoming the inherent slow kinetics of ring-opening reactions of turn-on photoswitches.

2. Results and Discussion

2.1. Synthesis and Characterization of BTCPO4s

Motivated by the above facts and limitations regarding the red-emitting BTCPO4 photoswitches, we synthesized a series of red-emitting BTCPO4 molecules (**7-13**). The BTCPO4s **7**, **8**, and **12** were reported in the literature, while the BTCPO4s **9**, **10**, **11**, and **13** were synthesized by us for the first time.[31,36,45] For varying the emission color, we changed the flanking aryl substituent at 6,6' position of the BTCPO4 moiety to extend the conjugation. The synthetic details and characterization of the BTCPO4 derivatives **7-13** are given in the SI (Scheme S1 and Figures S1–S16, Supporting Information). After synthesis and purification, the BTCPO4 molecules were isolated by column chromatography in the dark to obtain the open isomers (**7a-13a**), and their absorption spectra are shown in Figure 1b and Figure S17 (Supporting Information).

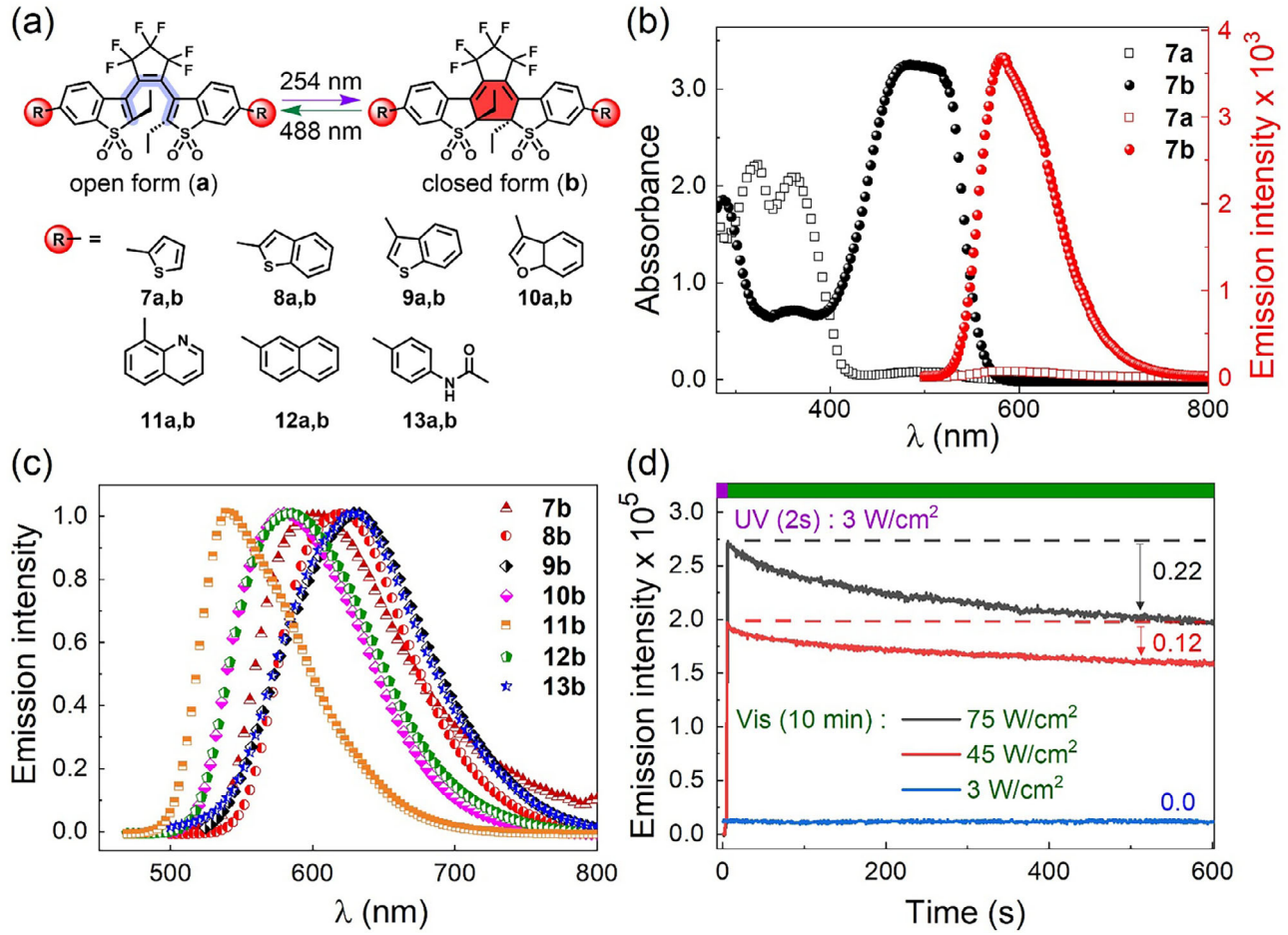

Figure 1. a) Schematics of photoswitching of BTCPO4 (open form) to BTCPO4 (closed form) in solution using UV (254 nm) and closed form to open form using visible light (488 nm) and the chemical structures of the different BTCPO4s; b) Absorption(black) and emission (red) of BTCPO4 **7** in the open form **7a** and closed form **7b** (λ_{ex} = 480 nm); c) Normalized emission spectra of closed forms of **7b**, **8b**, **9b**, **10b**, **11b**, **12b** and **13b** (λ_{ex} = 480 nm for **7b**, **8b**, **9b**, **10b**, **12b**, **13b** and λ_{ex} = 450 nm for **11b**); d) Photoswitching of **7a** blended with PPMA in thin film by using 325 nm UV (3 W cm^{-2}) to **7b** (violet) and with 488 nm from **7b** to **7a** at different intensities of 3 (blue), 45 (red) and 75 W cm^{-2} (black). The absolute starting emission intensities (at zero time) are different due to the different excitation intensities (VIS intensity) of each measurement ($I_{excitation} \sim I_{emision}$).

2.2. Absorption and Emission of BTCPO4s in Solution

First, the absorption and emission of BTCPO4s **7-13** with different substituents at 6,6' positions (**Figure** 1a) were studied in acetonitrile solutions. As a typical example, the spectra of **7a**,**b** are shown in Figure 1b. Figure S17 (Supporting Information) for the individual absorption and emission spectra of the other BTCPO4 molecules, (**8-13**). The open form of the **7a** has a characteristic absorption in UV below 400 nm. The negligible absorption in the visible range above 400 nm arises because of the small amount of the closed isomer present in the solution after synthesis. The solution of **7a** was irradiated with UV light (λ: 254 nm, 8 W) to convert it to the closed emitting form (**7b**) via a photoinduced cyclization reaction to **7b**. The conversion of open form **7a** to closed form **7b** can be easily distinguished by the change in the UV–vis absorption (in black) and emission spectrum (in red) of the molecule (Figure 1b). After UV light irradiation, the absorption shifts toward the visible region (400-700 nm). This shift is due to the extended π-electron delocalization in the closed isomer. Unlike the open ring isomers **7a-13a**, all the closed ring forms **7b-13b** are emissive; the emission spectra of the closed forms **7b-13b** are in the red spectral region from 550-750 nm (Figure 1c). The emission peak maximum (λ_{max}) varies over a broad range from 540 nm for **11b** to 740 nm for **9b** and **13b**. Except **11b** (with emission in the green region), all the rest six BTCPO4 molecules (**7b**, **8b**, **9b**, **10b**, **12b**, and **13b**) emit in the red region. This broad variation of emission was achieved by varying the flanking aromatic moieties as envisaged in the synthetic strategy.

2.3. Kinetics of Photoswitching of Red Emitting BTCPO4 in Thin Films

To study the photoswitching process of molecules **7-13**, we prepared thin films of all embedded in PMMA matrices on quartz coverslips (see SI for detailed procedure). The photocyclization reaction was then carried out by irradiation using 325 nm laser (3 W cm^{-2}) for 2s. These parameters of UV laser intensity and

duration were selected from our previous studies of green emitting photoswitches.[44] The reverse cyclization using 488 nm laser (at 3 W cm^{-2}) was found to be very slow, and therefore this step was repeated with increasing light intensities of 45 and 75 W cm^{-2} for up to 10 min. A typical example of photocyclization of non-emitting **7a** to the emitting isomer **7b** and its reverse cyclization to the open form **7a** is shown in Figure 1d. Photocyclization of **7a** to **7b** was fast (2s) as reported for BTCPO4s, while the conversion of the **7b** to **7a** was very slow. At a lower light intensity of 3 W cm^{-2} we did not observe the reverse cyclization of **7b** to **7a** at all, while at 45 W cm^{-2} we observed a partial ring opening with a contrast ratio C of just 0.12. Here, contrast ratio is defined as $C = 1 - \frac{I_{min}}{I_{max}}$; where I_{max} refers to the highest emission intensity of the sample that is observed at the beginning of Vis_{488} nm illumination, and I_{min} refers to the lowest emission intensity of the sample during 488 nm illumination at time t (here, $t = 600$ s). Irradiation at 75 W cm^{-2} did not speed up the conversion significantly and resulted in a slightly higher contrast ratio of 0.22. The photoswitching experiments with the same parameters were also carried out for all the BTCPO4 molecules in thin films (see Figure S18, Supporting Information). In each case, cyclization to the emissive forms **8b-13b** was very fast, whereas reverse cyclization at a high laser intensity (75 W cm^{-2}, 600s) was found to be very slow, and the achieved contrast ratios of C = 0.17 to 0.50) also were not very high, except for the green emitting molecule **11b** (C = 0.65). In summary, the reverse cyclization of the red emitters is 300 times slower than the cyclization reaction (600s vs 2s). However, for highly efficient writing-reading-erasing cycles involved in optical data encryption and possible data storage applications, both the cyclization (corresponding to writing data) and reverse cyclization reaction (corresponding to erasing) should be very fast.[44] By comparison, our previous studies on a green-emitting BTCPO4, which emits in the 550 nm range, showed a fast reverse cyclization (irradiation for 29s at 488 nm) at low power intensity of 3 W cm^{-2}, resulting in a very good contrast ratio of 0.85.[44] It is also equally important to have the fast-photoswitching processes at low intensity laser irradiation to maintain the high fatigue resistance and to avoid any sample damage. Thus, it is essential to address these fundamental issues to enable the application of red emitters with high fatigue resistance, long durability, and fast switching in both directions under low intensity of UV as well as visible light. In the following, we discuss a new strategy to achieve this.

2.4. Fast and Reversible Emission Modulation of Blends of DCP and Red Emitting BTCPO4 in Solution

It has been reported by us and others that non-emitting DCP derivatives can be switched back to open isomeric forms at a very fast rate with low intensity of visible light irradiation (100 mW cm^{-2}).[27,46] Therefore, we thought that it is worthwhile exploring the quenching of red emission of BTCPO4 by possible energy transfer (ET) processes to a non-emitting DCP isomer, which switches very quickly and changes its frontier energy orbital energy to facilitate ET processes. In this way, the emission can be switched off at a faster rate using low-intensity light instead of attempting to photoswitch the red-emitting BTCPO4s to their non-emissive forms. To verify our idea, first, we mixed the red-emitting BTCPO4 **7b** with the open form of non-emitting DCP **14a** in acetonitrile and irradiated this mixture with UV light (254 nm, 8 W). The non-emitting DCP **14** chosen here is well known for its fast photoswitching, high absorption coefficient at 600 nm in the closed form, high fatigue resistance, and thermal stability.[18] It has also been demonstrated that the DCP in closed form is capable of ET processes with red fluorescent dyes.[25–28] The schematics of photoswitching of DCP and possible red emission quenching/ modulation via ET are depicted in **Figure 2a**. The irradiation times and change in absorption of **14a** alone as a function of time (0–5 min) are shown in Figure 2b. It is obvious that **14a** converts to its closed form **14b** during prolonged irradiation with UV light (254 nm) as seen at the absorption of the closed isomer in the visible region (450–700 nm), increasing continuously with almost complete conversion in 3 min. The absorption peak at 600 nm, which is a characteristic peak of **14b** saturates after 3 min, suggesting that **14a** is fully converted to **14b** within 3 min of 254 nm irradiation (Figure 2b).[18] Also during the UV irradiation of the mixture (**7b +14a**) for a period of 5 min, a full ring closure of the **7b** occurs (absorption increase in the range of 400–550 nm) (Figure 2c). Simultaneously, the emission of **7b** in the mixture is progressively quenched during the ring closure of **14a** to **14b** in accordance with the PL measurement data (Figure 2d) and as indicated by the color change from red fluorescent to a non-fluorescent brown color (Figure 2a). A remarkably high maximum emission quenching of 95% was observed within 5 min UV irradiation of the mixture in solution. Further, the original intense red-fluorescent color was recovered from the non-fluorescent brown sample by irradiation with the 600 nm LED light (40 W), which enables the ring-opening of **14b** to yield the **14a** isomer, but not the conversion of 7b–7a (which is very slow as discussed above). Since the closed non-emitting **14b** has a very good absorption overlap with the emission spectrum of **7b**, it fulfils one of the basic requirements for an energy transfer process from **7b** to **14b**. Here, it is important to note that the absorption spectrum of the open isomer **14a** does not overlap with the emission spectrum of **7b** at all, and therefore, probably it cannot undergo any kind of energy transfer. This is manifested by the 100% recovery of emission intensity in **14a +7b,** and this process can be repeated multiple times in the solution in both directions (Figure 2e). To emphasize, we were able to achieve a high contrast ratio of 0.95 (95% emission quenching) and fast reversible switching of red emission in solution. We also carried out similar emission quenching experiments with the other mixtures **8b+14a**, **9b+14a**, **10b+14a**, **11b+14a**, **12b+14a,** and **13b+14a** in solution using UV and visible light irradiation. We observed a similar trend of high contrast ratio (0.80-0.95) as a function of UV light irradiation duration in acetonitrile (Figures S19–S25, Supporting Information).

2.5. Mechanistic Investigation of Emission Modulation of 7b+14a Mixture in Solution

The 95% emission quenching observed in the **7b+14a** mixture by switching **14a** to **14b** could be due to different reasons, such as electron transfer, non-radiative energy transfer (via Föster Resonance Energy Transfer FRET), or radiative energy transfer or a combination of these processes. It is known that the energetics

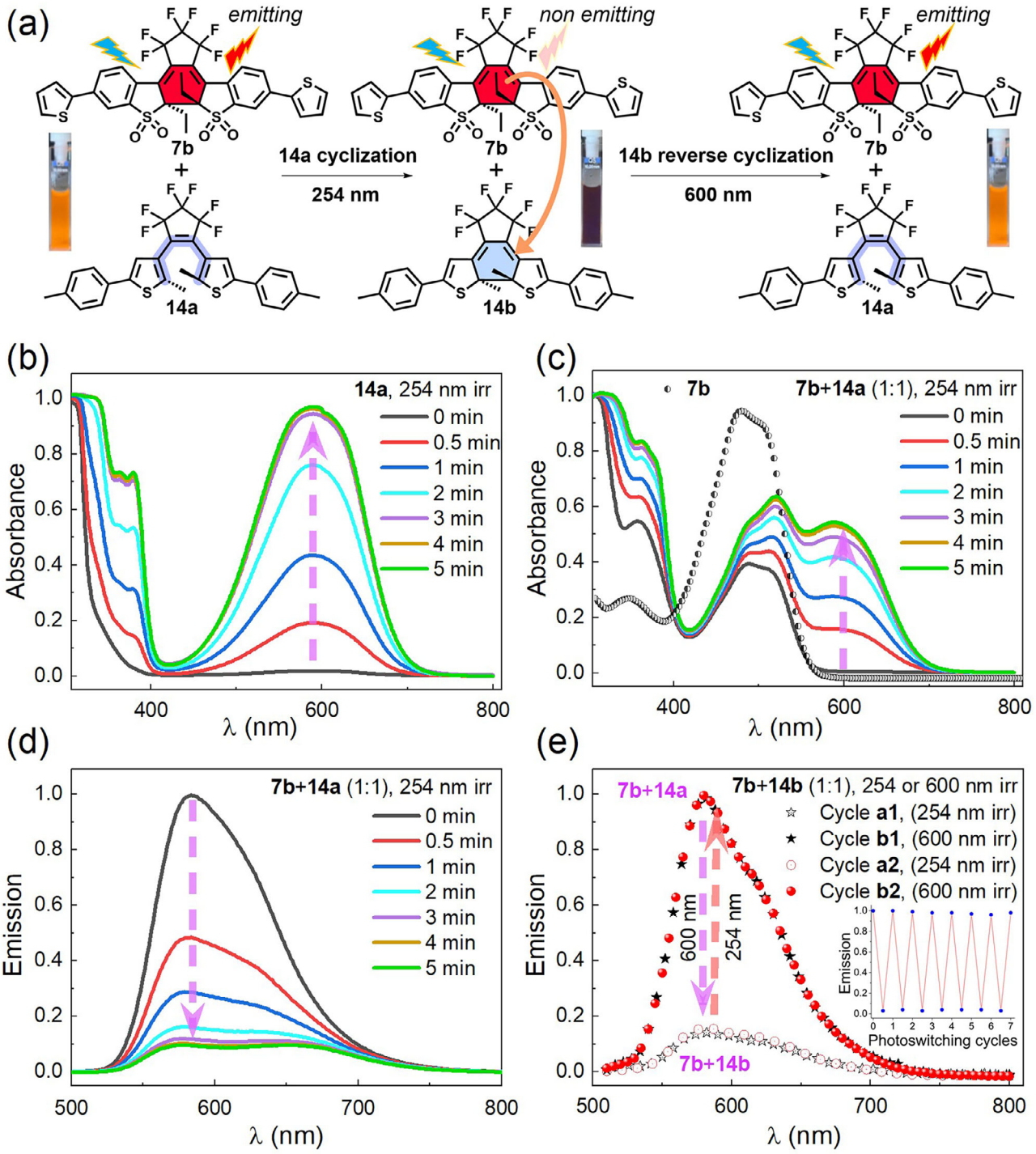

Figure 2. Absorption and emission study of **14a** and **7b**+**14a** (1:1) mixture (200 μM concentration of each) in acetonitrile using UV (254 nm, 8 W) for cyclization and Vis (600 nm, 40W LEDs) for ring opening. Emission spectra were recorded by λ_{ex} = 480 nm: a) Schematic representation of fluorescence modulation in a mixture of (**7b**+**14a**) and color change before and after UV and Vis light irradiation; b) Absorption spectrum of **14a** recorded at different irradiation time with 254 nm irradiation; c) Absorption spectra of **7b**+**14a** (1:1) recorded at different irradiation time with 254 nm; d) Decrease in emission intensity of **7b**+**14a** (1:1) at different time intervals of UV irradiation due to conversion of **14a** to **14b**; e) Reversible emission quenching for two photoswitching cycles of **7b**+**14a** (1:1), and in inset- seven photoswitching cycles of **7b**+**14a** (λ_{ex} = 480 nm).

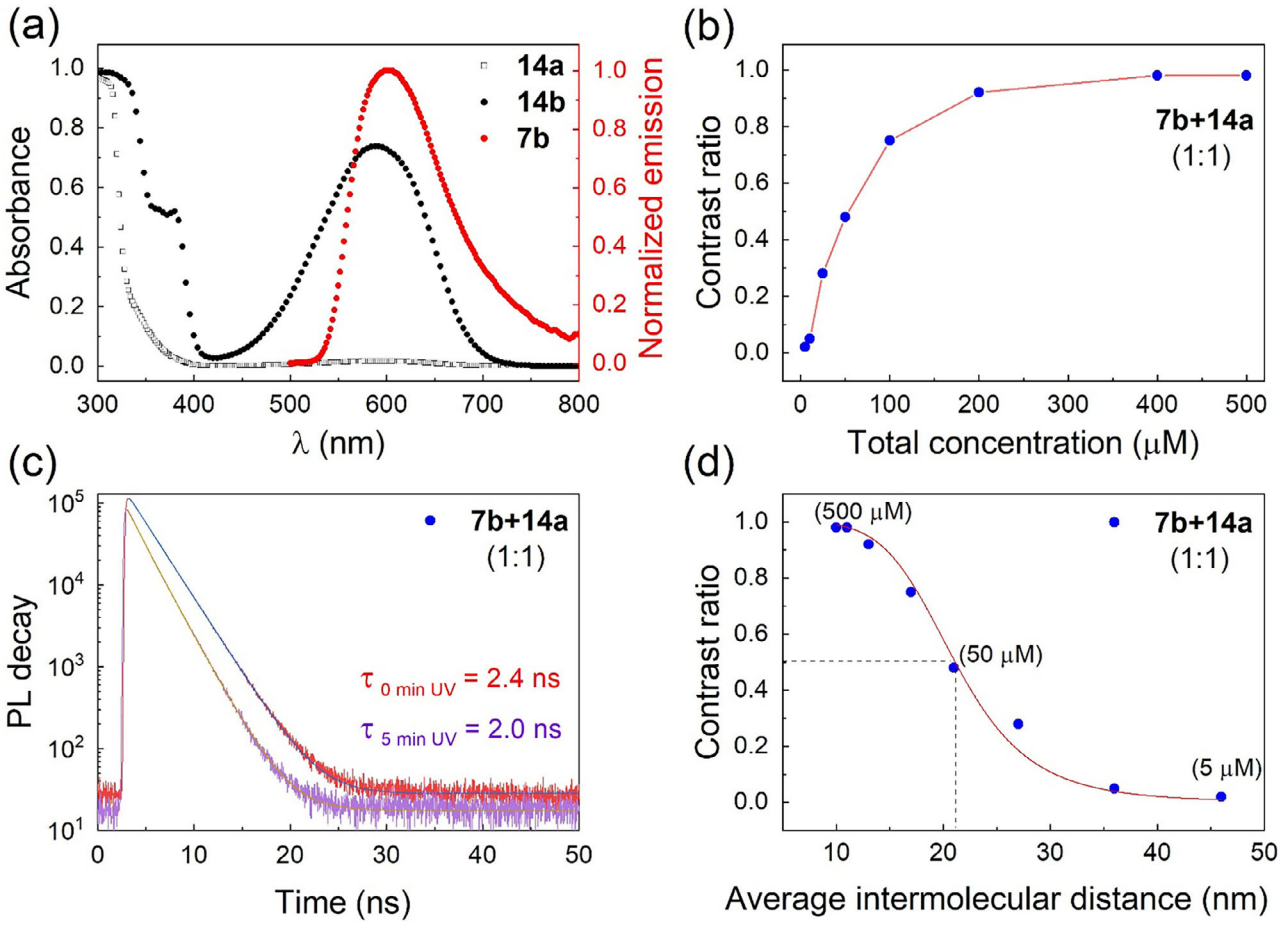

Figure 3. a) Absorption spectra of **14a** and **14b** overlapped with the emission spectra of **7b**; b) Concentration dependent contrast ratio plot of **7b**+**14a** (1:1) mixture in acetonitrile on UV irradiation (254 nm, 5 min); (after UV irradiation, **14a** gets converted into **14b** resulting in PL quenching); c) PL lifetime decay in acetonitrile before (**7b**+**14a**) and after (**7b**+**14b**) irradiation of 254 nm; d) Plot of contrast ratio against average intermolecular distance in the solution at different concentrations.

orbitals of **14 a** change drastically on UV irradiation, resulting in the closed form **14b**. Therefore, before investigating the emission quenching phenomenon, we calculated the HOMO-LUMO energy levels of all BTCPO4 (**7a**,**b**-**13a**,**b**) and DCP **14a**,**b** in both open and closed form by DFT (see Table S1, Supporting Information for all calculated orbital energy values). The LUMO energy values of closed form isomers, **7b**-**13b** (lie in the range of −3.18–−3.44 eV), are less than the LUMO energy value of the DCP in the open form **14a** (−1.78 eV) and closed form **14b** (−2.71 eV). These energy levels clearly suggest that electrons from the closed form of **7b**-**13b** to a high-lying LUMO energy level of **14b** are energetically unfavorable. Thus, the emission quenching by electron transfer can be almost ruled out. The obvious spectral overlap observed between the absorption spectra of **14b** and the emission spectra of **7b** (**Figure** 3a) implies that there are now two ET possibilities for emission quenching, namely: (FRET) or radiative energy transfer, or a combination of both. To understand the contributing factors and their mutual distance dependence in the ET process toward highly efficient quenching in the mixture in acetonitrile solution, we have performed PL quenching experiments with increasing concentrations (2.5 to 250 μM each) of both **7b** and **14a**, at a 1:1 molar ratio. Thus, the total concentration was varied from 5 μM to 500 μM. Here again contrast ratio, $C = 1 - \frac{I_{min}}{I_{max}}$, where I_{min} is the PL intensity measured after 5 min 254 nm irradiation, and I_{max} is the PL intensity measured before 254 nm irradiation. The obtained contrast ratio is plotted against the total concentration of the photoswitches **7b** and **14a** (Figure 3b). We observed an increase in contrast ratio with an increase in the concentrations of the **7b** + **14a** from 5 to 200 μM. At 200 μM concentration (100 μM of each), saturation of contrast ratio at ≈0.92 was observed. The increase in contrast ratio with an increase in total concentration can be explained by the possible decrease in average molecular distance between **7b** and **14b**. This result confirmed the molecular distance-dependent nature of PL quenching. Therefore, this implies that the emission quenching could be because of FRET. To verify the role of FRET, we carried out PL lifetime decay experiments on the mixture **7b**+**14a** before and after irradiation with 245 nm for 5 min, during which **14a** was converted to **14b**. (Figure 3c). The PL lifetime decay experiment showed a small decrease in the lifetime (τ) of emitting **7b** after irradiation of 254 nm for 5 min (from τ = 2.4 ns for **7b**+**14a** to τ = 2.0 ns for **7b**+**14b**). This decrease in lifetime indicates an energy transfer from **7b** to **14b**. However, this small change in lifetime of the excited state of **7b** (just 17% decrease in τ) may not explain the

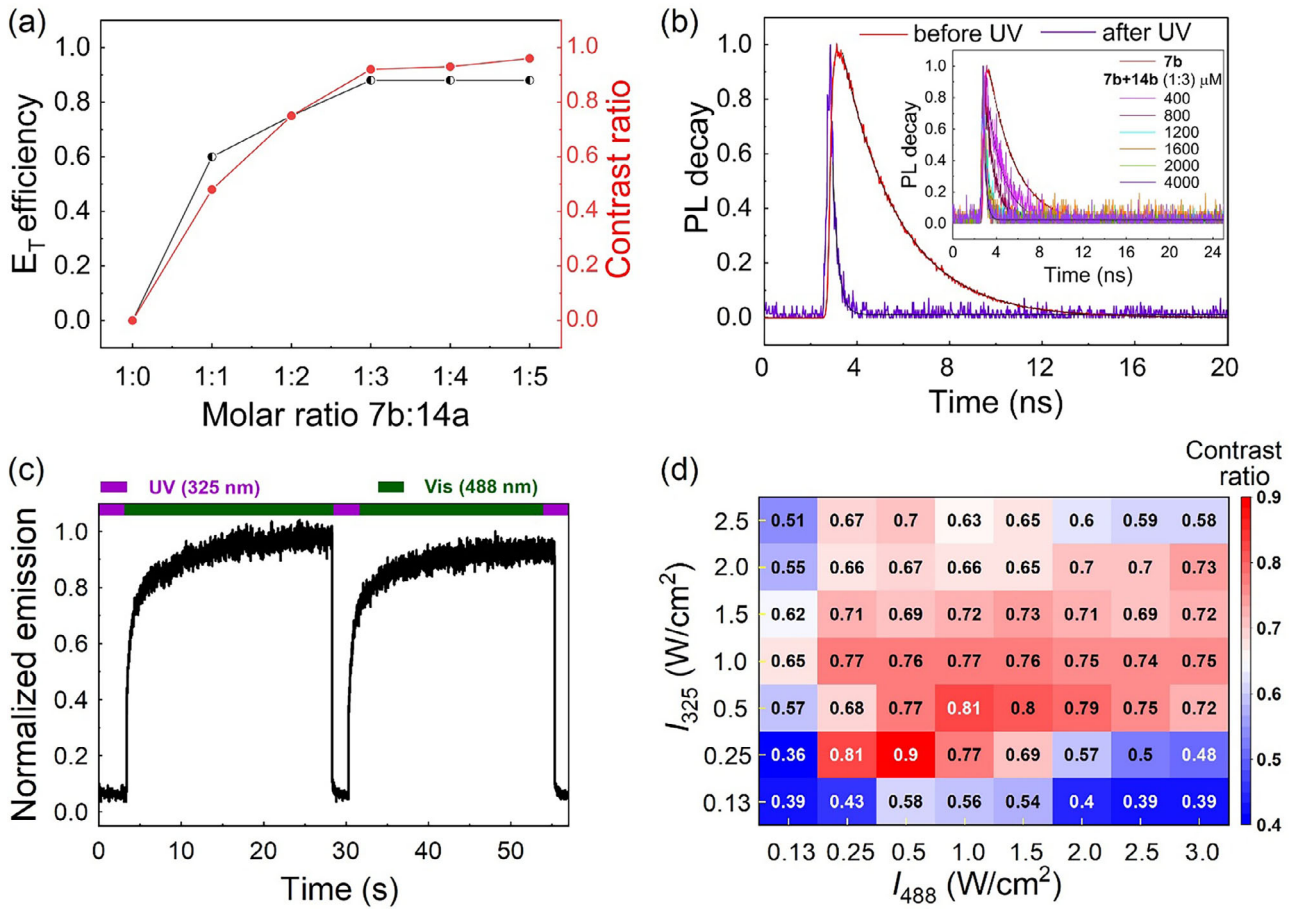

Figure 4. Photoswitching in PMMA film blended with (**7b**+**14a**) using 325 nm UV laser for 2s and 488 nm Vis laser radiation for 25s: (a) Energy transfer efficiency and contrast ratio in film samples with different molar ratios of **7b**+**14a**, (concentrations used for film preparation are: **7b,** 400 μM and **14a**, 0, 400, 800, 1200, 1600, 2000 μM respectively); b) PL lifetime decay of **7b**+**14a** (1:3 molar, 1600 μM), before UV irradiation (red) and after UV irradiation for 1 min (purple). Inset: PL lifetime decay of film samples of different concentrations; c) Photoswitching of **7b**+**14a** (1:3) using UV 0.25 and Vis 0.5 W cm^{-2}. The concentration used for film preparation **7b** is 400 μM and **14b** is 1200 μM; d) Contrast ratios (red: maximum and blue: minimum) for **7b**+**14a** (1:3) 1600 μM at different intensities of 325 nm and 488 nm.

very efficient PL quenching (contrast ratio 0.95) observed in solution. Thus, to further study any possibility of FRET (operating range of 1-10 nm distance) in this PL quenching process, we have calculated the average distance between the molecules in the solutions at different concentrations (Pages S23–S24, Supporting Information for calculations and the values). This average intermolecular distance arising out of the different concentrations is plotted against the measured contrast ratio of **7b** emission in the mixture **7b+14a** obtained after UV irradiation (Figure 3d).[47,48] The plot exhibits a sigmoidal curve, and the calculated intermolecular distance between the two molecules decreased from 46 nm to 10 nm with an increase in concentration from 5 to 500 μM, respectively. A 0.5 contrast ratio was observed at an average intermolecular distance of 21 nm. Further, the contrast ratio increased to 0.98 when the average intermolecular distance decreased to 10 nm for 500 μM concentration. Since FRET is effective only below an intermolecular distance of 10 nm, we can say that FRET is perhaps not a predominant factor for PL quenching observed in solution under these low concentrations.[49,50] Therefore, we increased the total concentration to 6 *m*M to verify the FRET contribution. At high concentrations, the influence of FRET was confirmed by calculating the FRET efficiency (E_T), as $E_T = 1 - \frac{\tau}{\tau_0}$, where τ is the lifetime of the mixture after UV irradiation (5 min UV) and τ_0 is the Lifetime of the pure emitting isomer **7b**. The lifetimes were obtained from the photoluminescence (PL) lifetime decay experiments of different samples of **7b+14a** with total concentrations ranging from 5 to 6 *m*M (Table S2, Supporting Information). The graph, E_T vs. intermolecular distance (Figure S26, Supporting Information), clearly shows that E_T increases considerably below 10 nm intermolecular distance, which corresponds to a total concentration of 500 μM. However, at 500 μM the FRET efficiency is less than 10% (Table S2 and Figure S26, Supporting Information). However, even at 6 *m*M concentration (≈4.3 nm), the calculated E_T was only 34%, even though >500 μM concentration, there is almost quantitative PL quenching (C = 98%). Additionally, we have quantitatively analyzed the Föster radius for 7b–14b donor-acceptor pair. The calculated radius is 5.51 nm (Pages S25 and S26 and Figure S27, Supporting Information for detailed calculations). To achieve this Föster radius in solution, the total concentration must exceed 3000 μM,

hence it clearly supports the possibility of FRET at higher concentration. However, we observed nearly complete PL quenching (C = 98%) at a much lower 400 μM concentration in solution (experimental concentration of 7b+14b, at a 1:1 molar ratio). This implies a strong possibility of radiative energy transfer of red emission of 7b to 14b due to the very good overlap of the emission spectrum of 7b with the absorption spectrum of 14b. The high absorption coefficient of 14b at 600 nm clearly favors the radiative energy transfer phenomenon as the dominant factor contributing to the observed high PL quenching in solution at experimental concentration (400 μM).

2.6. Red-Emission Modulation of the Blends of DCP and BTCPO4s in Thin Films (Solid State)

A further increase in intermolecular distance is feasible in the solid state, and many applications of optical data storage require thin film systems. Therefore, we prepared thin films of **7b+14a** mixture with PMMA as matrix, coated on a quartz substrate, and studied the PL quenching. During the film preparation, after spin coating, all solvent molecules evaporated completely. This leads to a significant reduction in intermolecular distances. As a result, we can expect enhanced emission quenching via FRET compared to solution samples. To validate this hypothesis, we studied the contrast of PL emission quenching and PL lifetime decay of thin film samples of the **7b+14a**. We also increased the stoichiometry of **7b**:**14a** (**7b**:**14a** = 1:1, 1:2, 1:3, 1:4, and 1:5 molar) to verify if a different molar ratio than 1:1 favors FRET. See Figures S28 and S29 and Table S3 (Supporting Information) for all the detailed results. The E_T and C values were plotted against the molar ratios of the **7b+14a** in **Figure** 4a. We observed a drastic increase in the contrast ratio from 0.48 to 0.96 in thin films as we increased the molar ratio of **14a** in the mixture from 1:1 to 1:5. At 1:3 molar ratio, the contrast ratio almost reached saturation. On the same line, we observed an increase in the energy transfer efficiency (E_T) from 0.60 to 0.88 and saturated as we increased the molar ratio of **14a** in **7b+14a** from 1:1 to 1:3. Thus, from Figure 4a it is very clear that the contrast ratio and the energy transfer efficiency values increase in equal magnitude suggesting that the emission quenching is predominantly because of the FRET process in the film samples. As typical examples, PL lifetime decay spectra of **7b+14a**, (at 1:3 molar ratio) before (red) and after UV irradiation (purple) are shown in Figure 4b.The lifetime of the sample **7b+14b** (sample after UV irradiation) is 0.3 ns, explaining also the very high energy transfer efficiency from **7b** to **14b** (E_T = 0.88) at this molar ratio of 1:3. In comparison, The lifetime of **7b+14a** (sample before UV irradiation) is 2.5 ns (exactly same as that of **7b** in PMMA film, τ = 2.5 ns), suggesting that there is no energy transfer from **7b** to **14a**. Further, we have also recorded the PL lifetime of the optimum mixture of **7b+14a** (at molar ratio 1:3) for different total concentrations ranging from 400 to 4000 μM (Figure 4b inset for spectra), to elucidate any influence of concentration at the optimum composition. The PL lifetime experiments showed an increase in energy transfer efficiency with an increase in total concentration from 400 μM to 1200 μM (**Table** 1). At 1200 μM, E_T saturated at 0.88, and it does not increase further on increasing concentration. A similar trend was also observed for the contrast ratio, with a clear rise and then a saturation at 1600 μM total concentration, as shown in Table 1. With this optimum sample concentration at 1:3 molar ratio (1600 μM), we performed red emission modulation of **7b+14a** with an UV_{325} laser light intensity of 0.25 W cm^{-2} for cyclization (writing) and a Vis_{488} intensity of 0.5 W cm^{-2} for reverse cyclization (reading and erasing).

Table 1. FRET E_T values and PL contrast ratio (C) for 7b+14a films prepared with different concentrations with molar ratios 1:3.

7b+14a (1:3) Concentration [μM]	τ after UV Irradiation [ns]	E_T 1 − $\frac{\tau}{\tau_0}$ [a]	C 1 − $\frac{I_{min}}{I_{max}}$ [b]
400	1.7	0.32	0.48
800	1.0	0.60	0.74
1200	0.3	0.88	0.91
1600	0.3	0.88	0.94
2000	0.3	0.88	0.95
4000	0.3	0.88	0.95

[a] τ_0 is the lifetime of **7b** in film (2.5 ns); τ is the lifetime of the sample after UV_{254} irradiation (1 min); [b] I_{max} = emission intensity of sample before UV_{254}; I_{min} = emission intensity of the sample after UV_{254} irradiation; Note- τ of sample **7b+14a** is exactly the same as τ_0 of **7b** (2.5 ns).

We achieved a fast writing with 2s, (for UV_{325}) and a fast erasing with 25s (for Vis_{488}) with a 0.90 contrast ratio (Figure 4c). Thus, this mixture **7b+14a** has clear advantages over **7b** alone, with 24 times faster erasing rate (erasing time decreasing from 600s to only 25s) and with an improved contrast ratio from 0.22 to 0.90 at lower visible light intensity (reduced from 75 to 0.5 W cm^{-2} of 488 nm). Here, the low intensity visible light of 488 nm played a dual role, on the one hand as an excitation wavelength for emitter **7b** and second as a trigger for the ring opening of **14b** to **14a**. The emission of **7b** at 600 nm can also assist the ring opening of **14b** to **14a**. In our earlier reports, we noted that specific combinations of UV and Vis laser intensities led to optimum contrast ratios in photoswitchable systems.[27,35,44] Therefore, we screened the influence of different laser intensity combinations of UV_{325} and Vis_{488} on contrast ratio to achieve the highest contrast ratio at the lowest UV/Vis intensities for a mixture of **7b+14a** (molar ratio: 1:3 at 1600 μM). The contrast ratios are depicted using a color code in Figure 4d, where red indicates the maximum and blue the minimum values. We obtained the highest contrast ratio of 0.90 at intensities of 250 mW cm^{-2} (UV) and 500 mW cm^{-2} for Vis light. In general, very low contrast ratios result if the laser light intensities are very low (130 mW cm^{-2}). Overall, we achieved a fourfold higher contrast ratio (0.90) for the **7b+14a** mixture using 150 times lower laser intensity (500 mW cm^{-2}) of Vis_{488} irradiation compared to (0.22) for **7b** alone (75 W/cm^2), as shown in Table S4 (Supporting Information). Notably, FRET-based emission quenching can be effectively achieved by preparing a film from a donor–acceptor mixture at a total concentration of 1600 μM or higher in a 1:3 molar ratio.

Further, we compared our results to our previous work based on the covalently linked non-emitting DCP with perylene bisimide as the fluorescent dye in a triad.[25] The covalent linkage of the bulky dye to the non-emitting DCP influenced the photoswitching parameters. Hence, a high laser intensity of visible irradiation (45 W cm^{-2}, 635 nm) was required for reverse cyclization of the DCP in triad. This visible intensity is 90 times

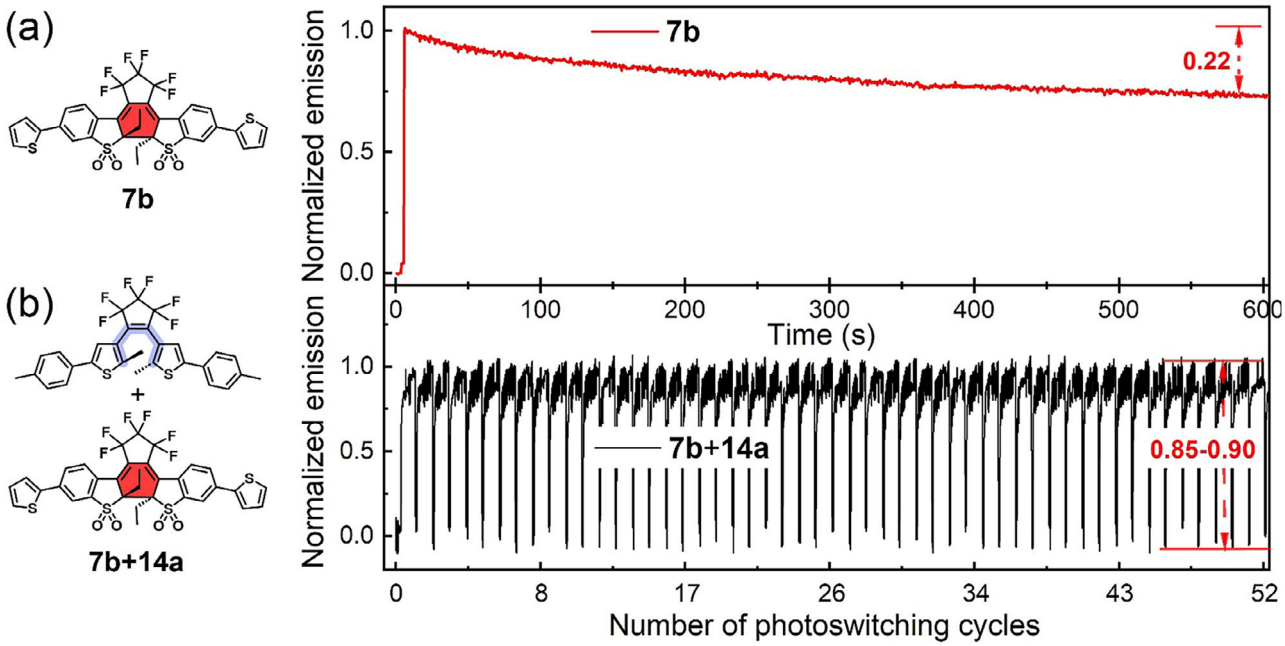

Figure 5. Comparison of photoswitching cycles: a) photoswitching cycle of 7a,b using UV 325 nm, 3 W cm^{-2} and Vis 488 nm, 75 W cm^{-2}; b) photoswitching cycle of 7b+14a using UV 325 nm, 250 mW cm^{-2} (1s) and Vis 488 nm, 500 mW cm^{-2} (10s).

higher than the visible intensity required for the emission modulation of the mixture **7b+14a**. Thus, this approach of mixing emitting BTCPO4 and DCP with accompanying FRET proved to be highly advantageous for fast reversible PL quenching or emission modulation of red emitters. To underscore, the demonstrated low laser intensities of UV and Vis are beneficial for future applications. With these optimized parameters for red emission modulation, we studied the emission modulation kinetics of other samples of red emitter mixtures such as: **8b+14a**, **9b+14a**, **10b+14a**, **11b+14a**, **12b+14a**, and **13b+14a** in thin films, and the results are summarized in Figure S30 (Supporting Information). All samples showed fast and reversible emission modulation with good contrast ratios of 0.85, 0.70, 0.82, 0.79, 0.73, and 0.90, respectively, in comparison to their corresponding emitting BTCPO4 **8b-13b** alone (Table S4, Supporting Information). The highest contrast ratio (0.90) was found for **13b+14a**, while the lowest (0.70) was found in the **9b+14a**. Among all the samples of mixtures, **7b+14a** (red emitting) and **11b+14a** (green emitting) are good candidates for future applications because of the high fluorescent quantum yields of the **7b** and **11b** (Table S4, Supporting Information).

Next, to check the fatigue resistance of reversible photoswitching of the **7b+14a** (1:3) blend film, we recorded multiple photoswitching cycles, from which the first fifty are shown in **Figure** 5. We observed a good contrast ratio between 0.85-0.90 even after 100 photoswitching cycles (Figure S31, Supporting Information), thus confirming the high fatigue resistance and good stability of this blend film under photoirradiation using Vis (488 nm, 500 mW cm^{-2}) and UV (325 nm, 250 mW cm^{-2}). A comparison of the red emission photoswitching kinetics of **7b** alone with that of the **7b+14a** blend film (Figure 5a vs 5b) demonstrates the superior fast switching behavior of the mixture unambiguously. We observed fast photoswitching (60 times faster, reduced from 600s to 10s), at low visible laser intensity irradiation (150 times lower, reduced from 75 to 500 mW cm^{-2}), and 4 times higher contrast ratio (from 0.22 in **7b** alone to 0.90 in the mixture).

2.7. Application of Smart Mixtures of DCP and BTCPO4s in the Solid State

To take advantage of the fast switching achieved in the blends, we examined their potential for optical information encryption. We considered **7b+14a** as a typical example to demonstrate this. For this, a well plate decorated uniformly with spherical microbeads coated with the photoswitchable mixture of **7b+14a** was tested for repeated write-read-erase cycles of the logo "AFUPO" using a mask and with UV light (254 nm) for writing, followed by visible light irradiation for reading and erasing as shown in **Figure** 6a–c. Further details of this demonstration are given in Section 6 and Figure S32 (Supporting Information). When irradiated with blue light, the optically written letters are read out in red color, while the other part of the sample does not emit (see Figure 6c). The letters were very bright and could be easily distinguished from the background due to the high contrast between the ON/OFF emission states. A complete erasing of the photowritten information was then achieved by irradiating the template with red light for 3 min. The template restored itself to its original state after information erasing (Figure 6a). In addition to fast photoswitching of emission, the mixture has another unique property, ie, it changes its color in response to irradiation with UV and visible light. So, we used this phenomenon to make color-changing objects, as demonstrated in Figure S34 (Supporting Information). These simple experiments demonstrate the feasibility of using

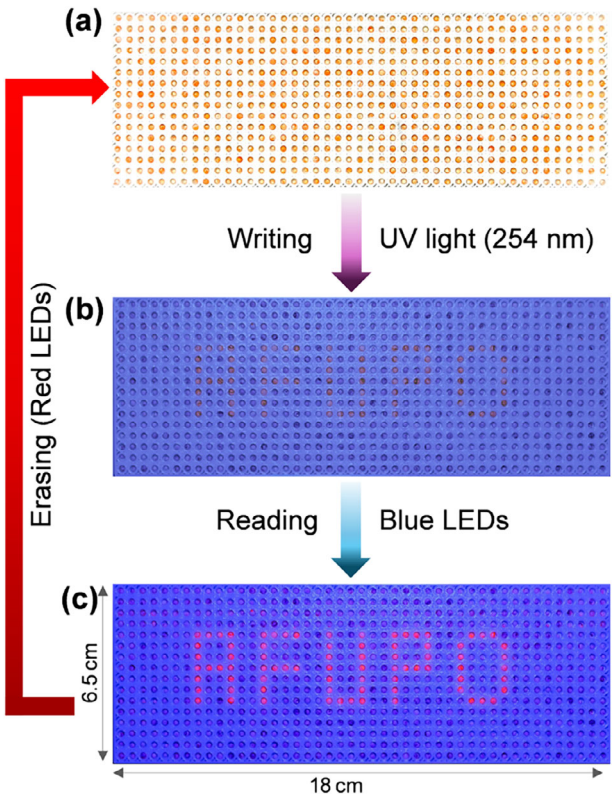

Figure 6. Information encryption on 3D-printed plate: a) Photograph of sample: **7b**+**14a** coated polypropylene granules arranged in an array of cavities of 3D printed PLA plate; b) Photograph of Sample under UV light: after writing the acronym "AFUPO" with UV 254 nm through a mask (1 min); c) Sample under blue LEDs: for reading the encrypted information.

write-read-erase cycles in photoswitchable molecules to store information.

3. Conclusion

We have synthesized and studied the photophysics of a series of new red-emitting photoswitches belonging to the class of BTCPO4. These red emitters are too stable in their closed isomeric form, and therefore the reverse cyclization is very slow, and it requires very high irradiation intensities and long illumination times. Moreover, the conversion efficiency is also very low. To overcome these issues, we have used a mixture of the emitting BTCPO4s (in their closed isomeric forms) and a non-emitting DCP to achieve the long-cherished goal of fast photoswitching of red emission. The strategy of mixing is very simple, and it avoids the tedious synthesis of complex molecules, in which the photoswitch must be covalently connected to the fluorophore. The PL lifetime decay data reveal that the main factor responsible for the quenching of the red emission of BTCPO4 (in closed form) by non-emitting DCP (in closed form) is via a radiative energy transfer process in solution; while, in the solid state, FRET is the predominant pathway for emission quenching. The reversible fast modulation of red emission was demonstrated at a low intensity of UV_{325} (250 mW cm^{-2}) and Vis_{488} (500 mW cm^{-2}) irradiation. Compared to BTCPO4 (**7b**) alone, the photoswitching of BTCPO4+DCP (**7b**+**14a**) mixture is 60 times faster, requires 150 times lower light intensity, and more importantly offers a four times higher contrast ratio (up to 0.90). The usefulness of the mixture was demonstrated for information encryption and to make the color-changing 3D printed objects that are sensitive to UV–vis light irradiation. Overall, this strategy allowed the very fast photoswitching of red emission in both directions with high fatigue resistance for the first time. Using this strategy, we realized that the fast-switching process of DCP molecule can be well exploited for radiative as well as non-radiative emission quenching. Also, FRET between the molecules is realized in thin films without covalently linking the molecules together, but instead simply by mixing them together above certain concentrations. Thus, the fast photoswitching of DCP molecule can act as a shutter between the input and output to modulate the red emission because of its high absorption coefficient at 600 nm. We also anticipate that the efficient red emission modulation achieved in these mixtures can be used for designing and addressing photonic circuits where the red-emitting mixture can act as an acceptor system and the light propagation can be modulated via non-emitting photoswitchable units.

Supporting Information

Supporting Information is available from the Wiley Online Library or from the author.

Acknowledgements

The authors thank Dennis Schröder and Jannik Petry for assistance with 3D printing of fullerene objects and 3D-plate with an array of micro-cavities. M.T. and J.K. thankfully acknowledge financial support by the Deutsche Forschungsgemeinschaft (Ko 1359/30-1, TH 807/11-1, GRK 2818) and the Bavarian State Ministry for arts and science within the initiative "Solar Technologies go Hybrid.". P.M. thanks the ARC for support through CE170100026.

Open access funding enabled and organized by Projekt DEAL.

Conflict of Interest

The authors declare no conflict of interest.

Data Availability Statement

The data that support the findings of this study are available in the supplementary material of this article.

Keywords

fast photoswitching, low laser intensity, red emission, turn-on photoswitches, writing-reading-erasing

Received: July 28, 2025
Revised: September 16, 2025
Published online: October 15, 2025

[1] S. W. Hell, *Science* **2007**, *316*, 1153.
[2] W. R. Legant, L. Shao, J. B. Grimm, T. A. Brown, D. E. Milkie, B. B. Avants, L. D. Lavis, E. Betzig, *Nat. Methods* **2016**, *13*, 359.
[3] A. A. Nagarkar, S. J. Root, M. J. Fink, A. S. Ten, B. J. Cafferty, D. S. Richardson, M. Mrksich, G. M. Whitesides, *ACS Cent. Sci.* **2021**, *7*, 1728.
[4] X. Wu, C. Barner-Kowollik, *Chem. Sci.* **2023**, *14*, 12815.
[5] D. Han, S. Yang, Q. Zhau, L. Zhan, S. Wan, Y. Deng, W. Li, *ACS Appl. Mater. Interfaces* **2024**, *16*, 10916.
[6] A. Goulet-Hanssens, F. Eisenreich, S. Hecht, *Adv. Mater.* **2020**, *32*, 1905966.
[7] I. M. Welleman, M. W. H. Hoorens, B. L. Feringa, H. H. Boersma, W. W. Szymański, *Chem. Sci.* **2020**, *11*, 11672.
[8] K. R. Sunil Kumar, T. Kamei, T. Fukaminato, N. Tamaoki, *ACS Nano* **2014**, *8*, 4157.
[9] G. C. Thaggard, J. Haimerl, K. C. Park, J. Lim, R. A. Fischer, B. K. P. M. Kankanamalage, B. J. Yarbrough, G. R. Wilson, N. B. Shustova, *Am. Chem. Soc.* **2022**, *144*, 23249.
[10] D. Roke, C. Stuckhardt, W. Danowski, S. J. Wezenberg, B. L. Feringa, *Angew. Chem., Int. Ed.* **2018**, *57*, 10515.
[11] Y.-Y. Tang, Y.-L. Zeng, R. G. Xiong, *Am. Chem. Soc.* **2022**, *144*, 8633.
[12] C. Zhang, H.-P. Zhou, L.-Y. Liao, W. Feng, W. Sun, Z.-X. Li, C.-H. Xu, C.-J. Fang, L.-D. Sun, Y.-W. Zhang, C.-H. Yan, *Adv. Mater.* **2010**, *22*, 633.
[13] J. C.-H. Chan, W. H. Lam, V. W.-W. Yam, *J. Am. Chem. Soc.* **2014**, *136*, 16994.
[14] M. Irie, *Chem. Rev.* **2000**, *100*, 1685.
[15] K. Matsuda, M. Irie, *J. Photochem and Photobio C* **2004**, *5*, 169.
[16] M. Irie, T. Fukaminato, K. Matsuda, S. Kobatake, *Chem. Rev.* **2014**, *114*, 12174.
[17] M. Irie, *Diarylethene Molecular Photoswitches: Concepts and Functionalities*, Wiley-VCH, Weinheim **2021**.
[18] M. Herder, B. M. Schmidt, L. Grubert, M. Pätzel, J. Schwarz, S. Hecht, *J. Am. Chem. Soc.* **2015**, *137*, 2738.
[19] F. Hu, M. Cao, X. Ma, S. H. Liu, J. Yin, *J. Org. Chem.* **2015**, *80*, 7830.
[20] G. Liu, C. Tian, G. Li, H. Zhang, X. Fan, L. Liu, Z. Cao, S. Jiang, X. Zheng, C. Niu, X. Xu, *ACS Mater. Lett* **2023**, *5*, 2299.
[21] M. Berberich, A.-M. Krause, M. Orlandi, F. Scandola, F. Würthner, *Angew. Chem., Int. Ed.* **2008**, *47*, 6616.
[22] M. Barale, M. Escadeillas, G. Taupier, Y. Molard, C. Orione, E. Caytan, R. Métivier, J. Boixel, *J. Phys. Chem. Lett.* **2022**, *13*, 10936.
[23] I. Ikariko, S. Kim, Y. Hiroyasu, K. Higashiguchi, K. Matsuda, T. Hirose, H. Sotome, H. Miyasaka, S. Yokojima, M. Irie, S. Kurihara, T. Fukaminato, *J. Phys. Chem. Lett.* **2022**, *13*, 7429.
[24] T. Fukaminato, T. Doi, M. Tanaka, M. Irie, *Chem. C* **2009**, *113*, 11623.
[25] M. Pärs, C. C. Hofmann, K. Willinger, P. Bauer, M. Thelakkat, J. Köhler, *Angew. Chem., Int. Ed.* **2011**, *50*, 11405.
[26] M. Pärs, K. Gräf, P. Bauer, M. Thelakkat, J. Köhler, *Appl. Phys. Lett.* **2013**, *103*, 221115.
[27] R. Schmist, M. Pärs, T. Weller, M. Thelakkat, J. Köhler, *Appl. Phys. Lett.* **2014**, *104*, 13304.
[28] J. Maier, T. Weller, M. Thelakkat, J. Köhler, *J. Chem. Phys.* **2021**, *155*, 14901.
[29] J. Maier, M. Pärs, T. Weller, M. Thelakkat, J. Köhler, *Sci. Rep.* **2017**, *7*, 41739.
[30] Y.-C. Jeong, S. I. Yang, K.-H. Ahn, E. Kim, *Chem. Commun.* **2005**, 2503.
[31] K. Uno, H. Niikura, M. Morimoto, Y. Ishibashi, H. Miyasaka, M. Irie, *J. Am. Chem. Soc.* **2011**, *133*, 13558.
[32] O. Nevskyi, D. Sysoiev, A. Oppermann, T. Huhn, D. Wöll, *Angew. Chem., Int. Ed.* **2016**, *55*, 12698.
[33] K. Uno, M. L. Bossi, M. Irie, V. N. Belov, S. W. Hell, *J. Am. Chem. Soc.* **2019**, *141*, 16471.
[34] B. Roubinet, M. Weber, H. Shojaei, M. Bates, M. L. Bossi, V. N. Belov, M. Irie, S. W. Hell, *J. Am. Chem. Soc.* **2017**, *139*, 6611.
[35] A. Albert, M. Fried, M. Thelakkat, J. Köhler, *Phys. Chem. Chem. Phys.* **2022**, *24*, 29791.
[36] O. Nevskyi, D. Sysoiev, J. Dreier, S. C. Stein, A. Oppermann, F. Lemken, T. Janke, J. Enderlein, T. Testa, T. Huhn, D. Wöll, *Small* **2018**, *14*, 1703333.
[37] J. Han, J. Zhang, T. Zhao, M. Liu, P. Duan, *CCS Chem* **2021**, *3*, 665.
[38] H. Zhang, M. Gießübel, P. Dharpure, A. Albert, V. Niestierkina, P. Mulvaney, M. Thelakkat, J. J. Köhler, *Adv. Funct. Mater.* **2025**, 2507180.
[39] Y. Takagi, M. Morimoto, R. Kashihara, S. Fujinami, S. Ito, H. Miyasaka, M. Irie, *Tetrahedron* **2017**, *73*, 4918.
[40] R. Iwai, M. Morimoto, M. Irie, *Photochem. Photobiol. Sci.* **2020**, *19*, 783.
[41] Y. Shi, J. Han, X. Jin, P. Duan, *Adv. Optical Mater.* **2022**, *10*, 2102180.
[42] R. Nishimura, E. Fujisawa, I. Ban, R. Iwai, S. Takasu, M. Morimoto, M. Irie, *Chem. Commun.* **2022**, *58*, 4715.
[43] H. Sotome, T. Nagasaka, T. Konishi, K. Kamada, M. Morimoto, M. Irie, H. Miyasaka, *Photochem. Photobiol. Sci.* **2024**, *23*, 1041.
[44] H. Zhang, P. Dharpure, M. Philipp, P. Mulvaney, M. Thelakkat, J. Köhler, *Adv. Optical Mater.* **2024**, *12*, 2401029.
[45] J. Han, J. Zhang, Y. Shi, P. Duan, *J. Phys. Chem. Lett.* **2021**, *12*, 3135.
[46] H. Jean-Ruel, R. R. Cooney, M. Gao, C. Lu, M. A. Kochman, C. A. Morrison, R. J. D. Miller, *J. Phys. Chem. A* **2011**, *115*, 13158.
[47] H. Paul, *Mathematische Annalen* **1909**, *67*, 387.
[48] H. P. Erickson, *Biol. Proced. Online* **2009**, *11*, 32.
[49] T. Förster, *Delocalized Excitation and Excitation Transfer. Modern Quantum Chemistry*, (Ed: O. Sinanoglu) Academic Press Inc, New York **1965**, p. 93.
[50] R. M. Clegg, *Fluorescence Resonance Energy Transfer. Fluorescence Imaging Spectroscopy and Microscopy*, (Eds: X. F. Wang, B. Herman) John Wiley & Sons Inc, New York **1996**, 179.